IMPROVEMENT OF DLR ROTOR AEROACOUSTIC CODE (APSIM) AND ITS VALIDATION WITH ANALYTIC SOLUTION

Jianping Yin, Jan Delfs

DLR, Institute of Aerodynamics and Flow Technology,
Technical Acoustics Division,
Lilienthalplatz 7, 38108 Braunschweig, Germany

Abstract

DLR's APSIM code was developed for prediction of rotor or propeller noise radiated in the free far-field. APSIM is the abbreviation for "Aeroacoustic Prediction System based on Integral Method". A new formulation based on airloads as input was derived and implemented in APSIM. The number of revolutions used in the input airloads can now be specified. This characteristic is very important for the tail rotor noise computation as the airloads on the tail rotor may not repeat after one revolution due to main and tail rotor interaction. The aeroacoustic results for the 40% scale BO105 main rotor and tail rotor configuration are calculated using both pressure distribution and airloads from DLR's UPM-Mantic code. The results using different aerodynamic inputs are compared. The implementation of the FW-H formulation based on penetrable surface into DLR's APSIM code is discussed. The aeroacoustic benchmark problems based on a point monopole source in various motions were used to validate the implementation. The comparisons were also made with Kirchhoff formulation. Finally, the effect of an open integral surface on the radiated sound field is discussed and suggestions on the future works are then presented.

1. Introduction

Helicopter is a versatile means of transport and fulfils increasingly a unique role in civil and military aviation, but a negative undesirable by-product of the helicopter during its operation is noise generation. The main sources of helicopter noise are its main rotor, tail rotor, engine, and the drive-train components. The dominant noise contributors are the main rotor and the tail rotor since they operate in free atmosphere and thus radiate noise unobstructed into the surroundings. With rising concern for environmental issues and increasingly stringent noise regulation, helicopter noise has gained importance in comparing with performance, safety and reliability.

A lot of progress has been made both in understanding the noise generation mechanism and in developing first-principle models for prediction of the noise. The computational aeroacoustics (CAA) and the approach based on integral formulation are now two commonly used noise prediction methods. CAA methods are designed to accurately capture the unsteady flow and noise radiation [1], but presently solving acoustic problems especially for 3-D rotor acoustic problems using CAA is still too expensive and unpractical. Therefore integral formulations, such as FW-H [2] and Kirchhoff formulation are still very useful in the rotor acoustic area.

Over the years DLR Institute of Aerodynamics and Flow Technology developed numerical tools [3,4] based on the integral Kirchhoff and the linear Farassat 1&1A methods [5] for prediction of rotor or propeller noise radiated into the free far-field. Afterwards to have a unique code for noise predictions of rotating blades the numerical tools were included in the code APSIM [6]. A validation of the code using the Kirchhoff and Farassat 1&1A methods were already presented in Ref. [7,8].

As part of using Farassat 1&1A method in which unsteady blade surface pressure data were required, APSIM was recently extended to include tail rotor noise computations using input data with more than one revolution [9], which is very important for the tail rotor noise computation as the airloads on the tail rotor may not repeat after one revolution due to main and tail rotor interaction. A formulation based on airloads as input was derived and implemented in APSIM [10,11]. The code has also been adapted to accept the blade pressure distributions from DLR's UPM-Mantic

(Main and tail rotor interaction code) [12] for the main/tail rotor interaction noise prediction.

As part of using aerodynamic field information, like Kirchhoff method, the FW-H formulation based on penetrable surface [13,14] or penetrable FW-H (P-FWH) formulation was implemented. The reasons for implementing P-FWH formulation are:

1. The Kirchhoff solution is very sensitive on the location of the integral surface, because the Kirchhoff method requires placing the integral surface in the region where the flow is completely governed by a homogeneous linear wave equation.
2. Current CFD simulation could only support information which is close to the source region where non-linear effect can not be avoided. The error due to non-proper location of the Kirchhoff surface can be large especially if the integral surface is positioned in the nonlinear region, even if in slightly nonlinear region.
3. P-FWH has all the advantage embedded in Kirchhoff formulation and is valid even if the integration surface is located in the nonlinear region and region containing vorticity so that it is less sensitive to the placement of the integration surface.
4. Input quantities are directly available from CFD codes, which is not the case for the Kirchhoff formulation.

The report is structured as follows. At first, the brief description on APSIM code is given. The extended APSIM code was applied to calculate the far field acoustic field radiated from a 40% scale BO105 main rotor and tail rotor configuration. The dependency of tail rotor aeroacoustic results on the different time length of the input data is presented. The computation results are compared. An aeroacoustic benchmark problem based on a point monopole source is then derived. This benchmark problem will be used to validate both P-FWH and Kirchhoff formulation and to identify non-appropriate integral surfaces. Finally, the effect of an open integral surface on the radiated sound field is discussed and suggestions on the future works are then presented.

2. Description of APSIM

The methodology of the APSIM is based on both FW-H and Kirchhoff formulations. The approach to compute noise radiation from helicopter rotors in the subsonic flow regime using DLR APSIM is split into two steps. In a first step, the aerodynamic flowfield is computed using an aerodynamics code. This then serves as input to APSIM which computes the acoustic pressure at any desired observer location. The aerodynamic code is kept as a separate program and is extended by an interface, which includes output routines to extract the pressure data of the flow field solution on special surfaces as required by APSIM.

Following improvements were made recently:

1. Main and tail rotor noise can be calculated and limiting requirements on the input data with one rotor revolution are removed;
2. The loading noise formulation based blade section lift was implemented;
3. P-FWH was implemented.

3. Application and validation

In order to test and verify new extensions or improvements based on Farassat 1 and 1A, a 40% scale BO105 main rotor and tail rotor configuration was used and unsteady blade pressure and load data were calculated by using DLR's UPM-Mantic code as well as CAMRA II (courtesy of ECD). A benchmark problem will be used to validate the P-FWH formulation.

3.1 Main rotor aeroacoustic results using different aerodynamic input

Under condition of potential flow, two different loading noise formulations were implemented, one (Farassat 1&1A) requiring unsteady pressure distribution on the blade surface and the other requiring unsteady blade section loads.

The loading noise based on unsteady blade section load or section lift l_f as the input is defined as:

$$4\pi p'_L(\vec{x},t) = -\frac{1}{c_0}\int_{F_m=0}\left[\frac{\dot{l}_f\,\hat{n}_i\hat{r}_i + l_f\,\dot{\hat{n}}_i\,\hat{r}_i}{c_0 r(1-M_r)^2}\right]_{ret} dl_{sp} -$$

$$\int_{F_m=0}\left[\frac{l_f(\hat{n}_i\hat{r}_i - \hat{n}_i M_i)}{r^2(1-M_r)^2}\right]_{ret} dl_{sp} -$$

$$\frac{1}{c_0}\int_{F_m=0}\left[\frac{l_f\hat{n}_i\hat{r}_i(r\,\dot{M}_i\,\hat{r}_i + c_0 M_r - c_0 M^2)}{r^2(1-M_r)^3}\right]_{ret} dl_{sp} \qquad (1)$$

The difference from the loading noise formulation of Farassat 1A is an analytical-integration in the chordwise direction, which was done in order to derive Eq.(1).

To test the validity of the loading formulation Eq.(1), the aerodynamic data calculated with the DLR's UPM-Mantic code were used.

The 40% scale BO105 main rotor and tail rotor configuration at 60 m/s level flight was simulated. The main rotor noise is then calculated using both unsteady blade pressure distributions and section lift respectively. Noise predictions are presented as contour plots (or footprints) of overall noise level and as time histories. The footprints are obtained in a representative sound field at 2.3 m below the main rotor hub which covers an area of one rotor diameter up- and downstream of the main rotor hub and laterally 1.1 rotor radii on either side of the hub. Since the rotor thickness noise can be obtained simply from the definition of the blade profile and motion and is independent on any aerodynamic inputs, the difference of rotor noise is purely caused by different aerodynamic inputs or loading noise.

The noise footprints under two different aerodynamic inputs are shown in Fig.(1). The circle and arrow in the figures represent the position of the main rotor and flow direction respectively. The comparison shows quite similar results both in noise directivity pattern and in general level.

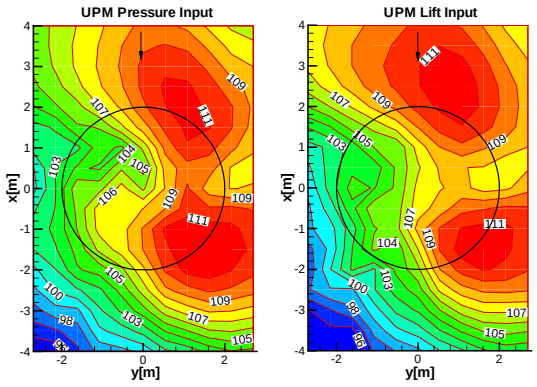

Fig. 1 Main rotor noise footprint for 60m/s level flight under two different aerodynamic inputs produced by UPM-Mantic (Overall sound pressure level(OSPL) in dB)

The comparisons are also made for sound pressure time histories for microphones at streamwise locations (Xmic = -2.0m). Fig.(2) illustrates the comparisons of the acoustic pressure-time histories with different inputs. The results are given for one main rotor revolution.

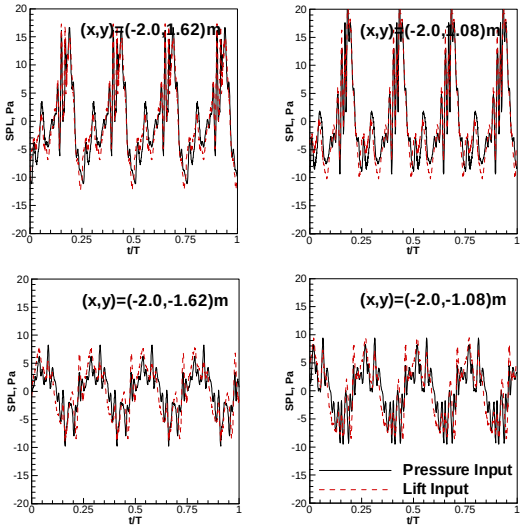

Fig. 2 Acoustic pressure time histories of sound radiated by main rotor for 60m/s level flight case at X=-2.0m, comparisons of two different aerodynamic inputs.

The comparisons on the acoustic time histories at different streamwise positions also prove that the implementation of new loading formulation is valid and effective.

3.2 Tail rotor aeroacoustic results using airloads with the time length of one or five revolutions

The 40% scale BO105 main rotor and tail rotor configuration again used for this study. The input airloads data is chosen from the ECD database for EU Heliflow Task5 pre-test computations simulated using CAMRAD II (courtesy of ECD). A 12 deg. climb case is used here, in which the tail rotor noise is important.

Fig.(3) shows the time history of the lift coefficient of the tail rotor blade versus several tail rotor revolutions at the different spanwise stations. The plots demonstrate very clearly that due to the existence of main/tail rotor interaction the lift coefficient varies with the revolutions. The repeat rate of the time history of the blade airloads depends on the ratio of main/tail rotor rotational speed, but in the acoustic computation, the repeat rate was assumed according to the time length of the input data. The minimum rate is one tail rotor revolution.

The tail rotor noise footprint as calculated using the blade airloads for two different number of revolutions are shown in Fig.(4). The footprints are given for an area located 2.3 m below the main rotor tip path plane. The time lengths of the input data are chosen corresponding to one and five revolutions respectively. The data within the dashline box as shown in Fig.(3) are selected if one revolution data input is used.

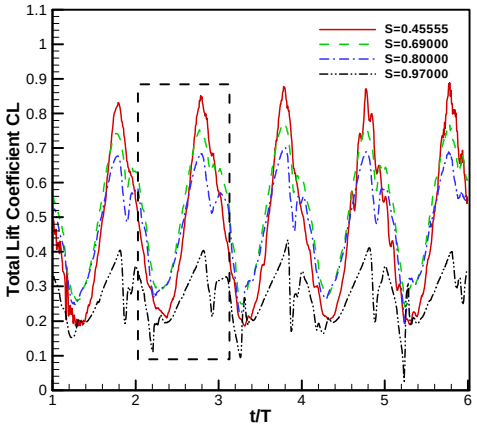

Fig. 3 The time history of section lift or airloads versus several tail rotor revolutions at different spanwise stations for the 12 deg. 33m/s climb.

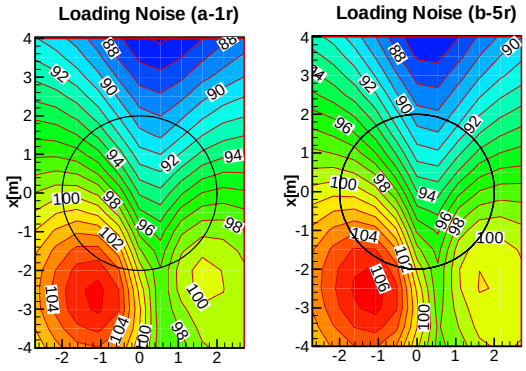

Fig. 4 Tail rotor loading noise, time length of input with (a) 1 revolution (b) 5 revolution (levels in dB) for the 12 deg. 33m/s climb.

The comparisons of the loading noise footprints as given in Fig.(4a) and Fig.(4b) show that although the footprints have quite similar noise radiation patterns, the differences in terms of magnitude in loading noise are obvious, especially in the area where the maximum noise radiation occurs.

Fig.(5) illustrates the comparisons of the acoustic pressure-time histories when different time lengths of inputs are used. The sound pressure time histories are selected from microphones at a streamwise location (Xmic = -2.5m) which coincides with the maximum noise radiation area. The comparisons are only made for the loading noise. The results are given for five tail rotor revolutions.

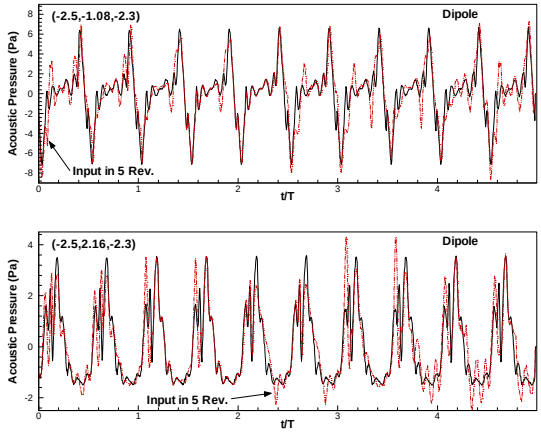

Fig. 5 Acoustic pressure time histories of loading noise at Xmic=-2.5m, comparisons of two different time lengths of inputs

The comparison with the results with different time length of input demonstrates that the

acoustic pressure time histories vary with the tail rotor revolutions. These variations are believed to be caused by the effects of main / tail rotor interaction. Input airloads over more revolutions are required if the main/tail rotor interaction effects are concerned.

4. Validation of P-FWH with an aeroacoustic benchmark problem

An aeroacoustic benchmark problem based on a point monopole source is defined. This benchmark problem will then be used to validate both FW-H and Kirchhoff formulation for a moving or a stationary integral surface. The advantages of using an analytical solution as a test bench for the validation are as follows:

1. the physical quantities can be obtained analytically on the integral surface so that any errors caused by preparing quantities on the integral surface using other numerical simulation can be avoided;
2. the effect of mesh size and wave number on numerical results can be studied without considering possible error from input data;
3. any error in the coding can be easily identified by code developers.

4.1 Exact solution for a moving point monopole source

Consider a point monopole (volume flow) source moving subsonically along the path $\vec{x} = \vec{x}_s(t)$ through an infinite medium that is otherwise at rest. The volume source density (volume flux) is then given by $Q(\vec{x},t) = q(t)\delta(\vec{x} - \vec{x}_s)$. The generated sound field is governed by

$$\frac{1}{c^2}\frac{\partial^2 p'}{\partial t^2} - \nabla^2 p' = \rho_0 \frac{\partial}{\partial t}[q\delta(\vec{x} - \vec{x}_s)] \tag{2}$$

After using the free field Green's function and making some mathematical manipulation [9], the solution for the potential φ, with $p' = -\rho_0 \frac{\partial}{\partial t}\varphi$, is given by

$$\varphi = -\left[\frac{q}{4\pi R(1-M_r)}\right]_{ret} \tag{3}$$

Where the subscript ret denotes evaluation at retarded time τ, given by the equation

$$t - \tau - \frac{R(\tau)}{c_0} = 0 \tag{4}$$

Where $R(\tau) = |\vec{x}(t) - \vec{x}_s(\tau)|$ so that τ is a function of t and x. M_r is the Mach number of the source movement in radiation direction.

After differentiating Eq.(3) with respect to time t, the acoustic pressure received at time t by an observer located at x is

$$p'(\vec{x},t) = \frac{\rho_0}{4\pi}\left\{\frac{1}{R(1-M_r)^2}\left[\dot{q} + \frac{q\vec{R}\bullet\dot{\vec{M}}}{R(1-M_r)} + \frac{qc_0(M_r - M^2)}{R(1-M_r)}\right]\right\}_{ret} \tag{5}$$

Where $\vec{M}$ and M are the vectorial and scalar Mach number of the source. The acoustic signal is radiated from a monopole source at retarded time τ and position $\vec{x}_s(\tau)$.

In order to prepare analytical quantities on the integral surface for both FW-H and Kirchhoff formulation, the perturbation velocity $\vec{u}$ and pressure gradients $\nabla p'$ are required. The $\vec{u}$ and $\nabla p'$ can be obtained by using

$$\vec{u} = \nabla\varphi = \nabla\left[\frac{-q}{4\pi R(1-M_r)}\right]_{ret}$$

$$\nabla p' = \frac{\rho_0}{4\pi}\nabla\left\{\frac{1}{R(1-M_r)^2}\left[\dot{q} + \frac{q\vec{R}\bullet\dot{\vec{M}}}{R(1-M_r)} + \frac{qc_0(M_r - M^2)}{R(1-M_r)}\right]\right\}_{ret} \tag{6}$$

The evaluation of Eq.(5) and Eq.(6) is carried out in retarded time frame.

4.2 Numerical procedure used to make code validation

The numerical procedure used to carry out code validation by using a point monopole source can be divided into following steps:

1. Constructing the integral surface enclosing the monopole source;
2. Computing the values of the physical quantities (depending on integral formulation) on the node point of given integral surface with Eq.(5) and Eq.(6);
3. Using quantities on integral surface prepared in step 2 as input into APSIM .

The monopole source with simple harmonic time dependence, $q(t) = Ae^{-i2\pi ft}$ is chosen in following simulations, where f and A are the frequency and the amplitude of the source respectively. A = 0.001 is used in the following validation cases. The integral surfaces are composed of one cylinder surface plus two end caps and each with 71 x 19 grid nodes. The total number of time steps is taken as 128 in the rest of computations. Both the radius and length of the cylinder are equal to 1.0m. The integral surface and its orientation are given in Fig.(6).

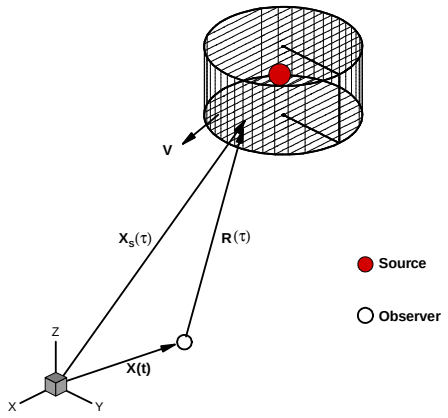

Fig. 6 The orientation and relation among the integral surfaces, observer and the source

Two types of source motions are involved in following validation cases, one with the source in purely straightforward translating motion at velocity $\vec{V}_0$ (30m/s) and the other with the source in both translating $\vec{V}_0$ and rotating motion. In both cases, the integral surfaces always translates with the observer at a speed of $\vec{V}_0$ in the x direction, as shown in Fig.(6). The situation of both observer and the surface translating together simulates a fixed microphone in a wind tunnel. The observer positions are located in a field which is at 2.3 m below the source and covers an area of $8 \times 4\,(\mathrm{m}^2)$.

4.3 Validation with the monopole source in simple translating motion

The source moves synchronously with the surface. There is no relative motion between the source and the integral surfaces.

Fig.(7) gives the comparison of the footprint between the predictions using P-FWH method and exact solution. The results using the Kirchhoff part of APSIM code are also presented in this plot. The far-field acoustic results compare almost perfectly with an exact analytical solution in terms of directivity.

The time histories at the observers selected along a cut through y = 0 are given in Fig.(8). The time history is plotted against one period of the signal. In order to look at the differences between the predictions and exact results, the part enclosed in a dashed line box in Fig.(8) is

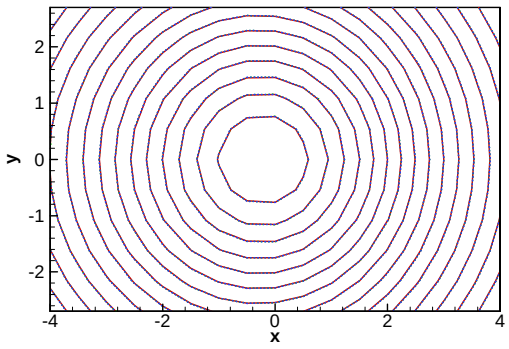

Fig. 7 Comparison of calculated acoustic pressure contour with exact, solution for a 70Hz moving mono-pole source, solid line (exact solution), and dashed line from P-FWH and Kirchhoff method.

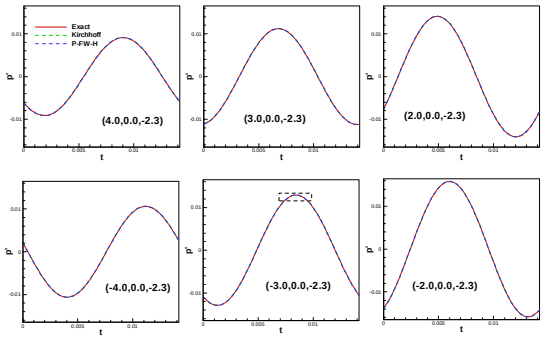

Fig. 8 Comparison of calculated time history of acoustic pressure with exact solution for a 70Hz moving mono-pole source, solid line (exact solution), dashed line from P-FWH and Kirchhoff method.

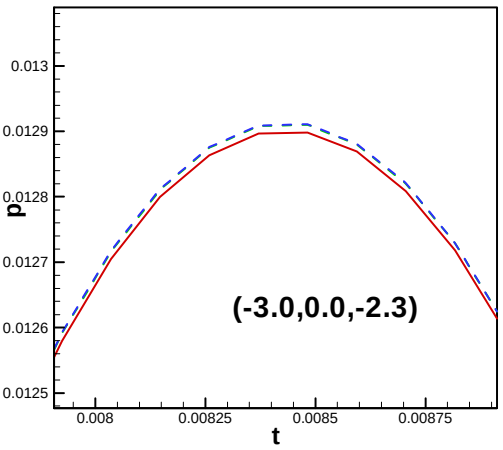

Fig. 9 Enlarged part of the time history in Fig.(4), solid line (exact solution), dashed line from P-FWH and Kirchhoff method.

enlarged and is given in Fig.(9). Little difference between two prediction results is observed because of the linear characteristics of the monopole source. Fig.(10) shows that the prediction results converge toward the analytical solution with doubling surface nodes.

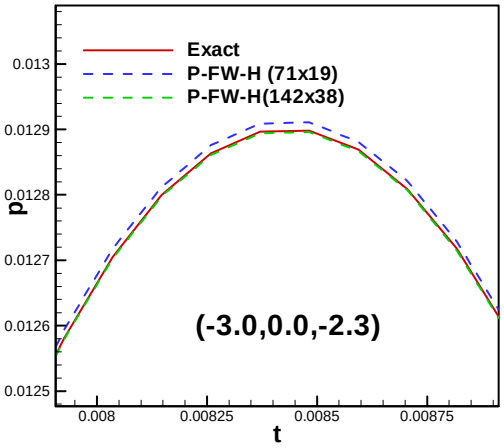

Fig. 10 Enlarged part of the time history in Fig.(4), solid line (exact solution), dashed line from P-FWH at two node points

4.4 Validation with the monopole source in both translating and rotating motion

The source is rotated around the center line of the surface in a radius of $R = 0.5(\mathrm{m})$ in addition to its translation with $\vec{V}_0$. The rotational speed of the source is 1050 RPM.

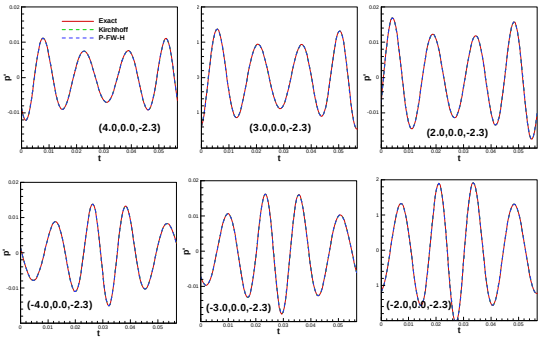

Fig. 11 Comparison of calculated time history of acoustic pressure with exact solution for a 70Hz rotational mono-pole source, solid line (exact solution), dashed line from P-FWH and Kirchhoff method.

The time histories at the observers defined in previous section are given in Fig.(11). The time history is plotted against one rotational period of the source, which is 4 times of the source signal period. The results compare quite well with the exact solution in terms of the amplitude and phase. The frequency and amplitude are modulated in the rotational period due to the relative motion (Doppler effects) between the source and the observer.

5. Identification of non-appropriate integral surface

As mentioned in previous section, the purpose of validation using the analytical solution is to avoid the errors due to other numerical factors, such as the error generated by converting data from CFD results, etc. Another important point is that any non-appropriate integral surface can be easily identified after running the proposed validation case. Fig.(12) shows three orientations of the integral surface which was subtracted from a CFD computation grid and used as a test case in APSIM previous Kirchhoff version. The integral surface is composed of 4 sub-surfaces. It can be seen very clearly that the sub-surfaces are not properly closed, which are required by the integral methods. The open area is marked as a and c in Fig.(12). The validation case described in 4.3 was repeated here.

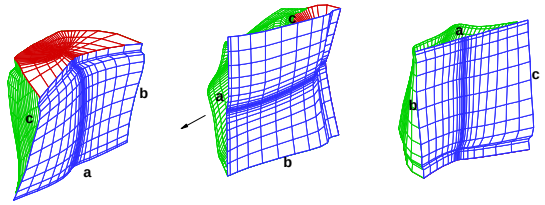

Fig. 12 Integral surface which was subtracted from CFD computation grid in different orientation, open areas are marked as a and b.

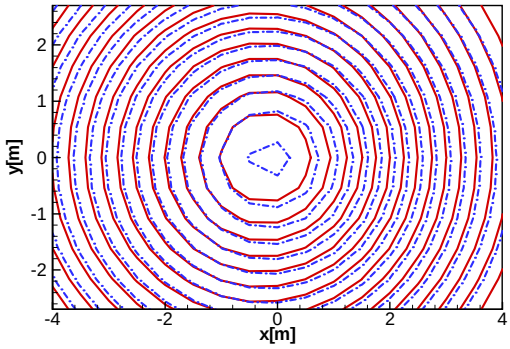

Fig. 13 Comparison of calculated acoustic pressure contour with exact, solution for a 70Hz moving mono-pole source, solid line (exact solution), dashed line from P-FWH using surface defined in Fig.(12)

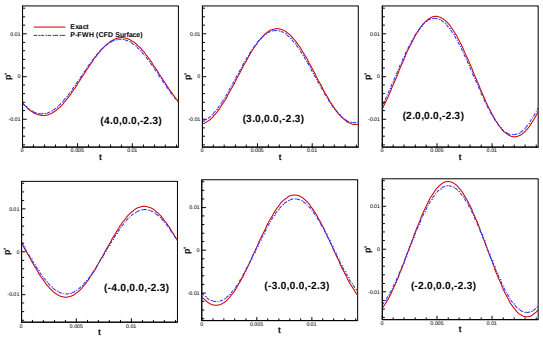

Fig. 14 Comparison of calculated time history with exact solution for a 70Hz mono-pole source, solid line (exact solution), dashed line from P-FWH using surface defined in Fig.(12).

Fig.(13) shows the comparison of predicted contour plots (using P-FWH method) and exact solution. The results using Kirchhoff method are the same as using P-FWH and not presented in the plots. Fig.(14) demonstrates the comparisons of the time histories at the observers position as defined in 4.3. The prediction errors are very obviously not only in magnitude but also in noise directivity. It is believed that the errors can be reduced by reducing size of the holes.

In this section, it has been demonstrated that the proposed benchmark problems can help to identify whether the integral surface is appropriate for the computation or not.

6. Calculation of sound field using an open integral surface

As pointed out by many authors, such as in [13,14], when using integral formulation based on Kirchhoff method, it is very important to place the integration surface in the region where the flow is completely governed by a homogeneous linear wave equation. But sometimes it is impossible to avoid any non-linear region to pass across the integral surface, such as rotor wake and especially the mixing layer or jets, if a closed integral surface enclosing a source region is required. This is, because of the limitation of the computing resource. The current CFD simulation could only provide information which is very close to the source region where non-linear effect can not be avoided. Therefore, an artificial opening on the integral surface is suggested in [16] to escape the strong non-linear region or the region where the acoustic portion of flow can not be separated out. But the opening also

removes a part of the linear wave which will make a contribution to the acoustic far-field. In addition, even with the P-FWH method, the subtraction of the surface from CFD results can hardly avoid any gap (opening area), such as the example demonstrated in the previous section, although P-FWH is valid even with the integral surface passing across a non-linear region.

In this section, the effect of an open integration surface on the radiated sound field is studied. The cylinder surface with two opening ends is used as shown in Fig.(15) in the following study. The diameter of the cylinder and mesh size on the cylinder is fixed in the simulation as defined in section 4.3.

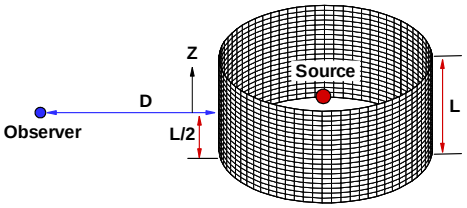

Fig. 15 Open integration surface

The static monopole source is used to generate the values required by the integral formulation on the integration surface. Two signal frequencies are chosen here, one is 70(Hz) and the other is 490 (Hz). The observer is located on the line which is on the symmetrical plane. The distance between the observer and the integration surface is defined as D=4.0. In order to avoid the influence due to different surface grid size, the surface grid size is kept constant while changing the length of the cylinder L.

Fig.(16) gives the time history of the acoustic pressure received at the observer position versus the different L and frequencies and their comparisons with the exact solution. With increasing L, the solutions converge to the exact solution not only in the amplitude, but also in the phase. Fig.(17) shows the errors for both amplitude and the phase relative to the exact solution versus the cylinder length. The difference of the phase is calculated according to the time difference of both calculated and exact solution at the signal peak position.

Fig.(17) demonstrates that the phase converges faster than the amplitude especially in the high frequency range, while the length of the cylinder required to get the same accuracy in the amplitude is almost the same in both frequencies. To prove that the oscillation in the convergence curve is not due to symmetry of the observer position with respect to the integral surface, a new computation is made for the observer with an off-set in Z direction. Z is defined in Fig.(15). The comparison of the result with and without off-set is given in Fig.(18). The characteristics of the convergence curves are almost the same.

It has been demonstrated in this section that the relations between the converged results and length of the open surface is frequency dependent. Therefore the caution is required in using the open integration surface even for a very simple source as used here.

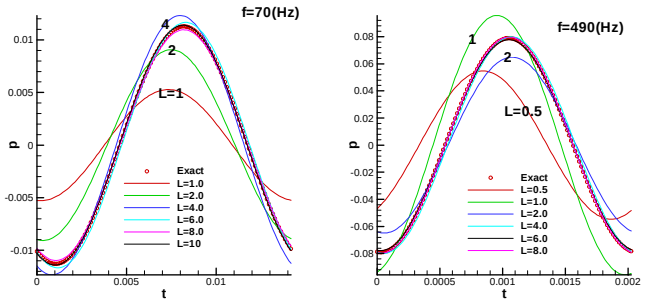

Fig. 16 the time history of the acoustic pressure received versus the different L and frequencies.

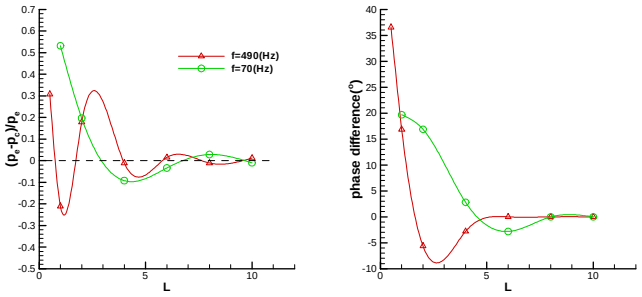

Fig. 17 The convergence rate versus the different L and frequencies.

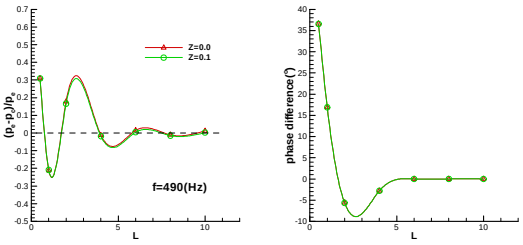

Fig. 18 The comparison of the convergence results with and without the observer off-set at the frequency f=490(Hz).

9. Future works

Following works will be carried out in the future development of the prediction tools, APSIM.

Validation of P-FWH using real life problems such as rotor noise by using the CFD computational results as an input;

Possible combination of CAA [1] and integral methods in order to benefit from the respective advantages of those methods.

Acknowledgement

The authors would like to acknowledgement the computed data obtained from ECD.

References

1. Delfs, Jan.: “SWING: A German Research Initiative into the Computation of Airframe Noise”. Proceedings Aeroacoustics Workshop, IAS, TU Dresden, Oct. 1999.
2. Ffowcs Wiliams, J., Hawkings, D.: “Sound Generation by Turbulence and Surfaces in Arbitrary Motion”, Phil. Trans. Roy. Soc. A264, 1969.
3. Schultz, K., Lohmann, D., Lieser, Pahlke, K.: “Aeroacoustic Calculation of Helicopter Rotors at DLR“, AGARD Fluid Dynamics Panel Symposium on Aerodynamics and Aeroacoustics of Rotorcraft, Paper N. 29, 1994.
4. Yin, J., ,Ahmed, S.,: ”Prediction- and its validation of the acoustics of multi-blade rotors in forward flight utilizing pressure data from a 3d free wake unsteady panel method', 20th European rotorcraft forum , paper no.11, October 4-7,1994, Amsterdam, the Netherlands.
5. Farassat:, F., “Linear acoustic Formulas for Calculation of Rotating Blade Noise“, AIAA journal 19, 1122-1130, 1981.
6. Kuntz , M. : “Aeroacoustic Program System APSIM, User Handbook, Release 5.2”, April, 2000.
7. Kuntz, M.,: “Ein nichtlineares aeroakustisches Verfahren zur Lärmvorhersage für Hubschrauberrotoren im Vorwartsflug“, DLR Forschungsbericht 1999-29, 1999.
8. Enrico Chelli: “Numerical Simulations of Noise Generated by a Helicopter Rotor in Descending Flight Condition Solving the Integral Farassat 1&1A Equations”. DLR IB 129-2000/8, Braunschweig, 20.04.2000
9. Yin, J. ‘Acoustic Prediction Using Ffowcs-Williams/Hawkings Formulation Based on CAMRAD Aerodynamic Airload Input’ DLR 129-2001/17, Braunschweig, 25.09.2001.
10. Pahlke, K.: “ECD/DLR Abstimmungs-gespräch ‘APSIM’ ”, Protokoll, BS, Jun. 2001.
11. Yin, J., “Status report on further improve-ments of APSIM-E’ DLR 129-2002/26, Braunschweig, 23. August 2002.
12. Yin, J., Ahmed, S.: “Helicopter main-rotor/ tail-rotor interaction', Journal of the American helicopter society”, Vol. 45, No. 4, pp293-302, October 2000
13. Di Francescantonio : “A New Boundary Integral Formulation for the Prediction of Sound Radiation” , Journal of Sound and Vibration (1997) 202(4), 491-509.
14. Brentner, K. S.; Farassat, F.: “ An Analytical Comparison of the Acoustic Analogy and kirchhoff Formulation for Moving Surfaces”, AIAA Journal, Vol.36, No.8,1998, 1379-1386.
15. Goldstein M..: “Aeroacoustics”, McGRAW-HILL International Book Company,1976.
16. Freund, J.B., Lele, S.K., and Moin P. : “Calculation of the radiated Sound Field Using an Open Kirchhoff Surface”, AIAA Journal, Vol.34, No. 5, May 1996.